PARABOLA III: a sphere-scanning radiometer for field determination of surface anisotropic reflectance functions

Carol J. Bruegge, Mark C. Helmlinger, James E. Conel, Barbara G. Gaitley, Wedad A Abdou

Jet Propulsion Laboratory, California Institute of Technology, Pasadena, CA 91109

ABSTRACT

The Portable Apparatus for Rapid Acquisition of Bidirectional Observation of the Land and Atmosphere III (PARABOLA III) is a sphere-scanning radiometer custom designed and built by Sensit Technologies, Inc. (Portland, ND). The original PARABOLA was built to study the relationship between surface morphology and reflected radiation properties. Follow-on work led to the design of an improved radiometer, the PARABOLA III. Two such instruments have been assembled, including one for the Jet Propulsion Laboratory. This in-situ sensor will be used to validate surface reflectances at angles measured by the Multi-angle Imaging SpectroRadiometer (MISR), a global imager flown on the Earth Observing System (EOS)-Terra orbital spacecraft. Derived PARABOLA III data products include the surface bidirectional reflectance factor, and sky and surface radiances for the upward and downward viewing hemispheres. This paper describes the design, calibration, and operation of the JPL PARABOLA III.

1. INTRODUCTION

With the advent of a new generation of calibrated, global multi-angle instruments, a rich data set is now available to apply to traditional remote sensing objectives, as well as to the study of Earth's climate and mechanisms which may lead to climate change. One such orbital sensor is the Multi-angle Imaging SpectroRadiometer (MISR), launched December 18, 1999 on-board the Earth Observing System (EOS)-Terra spacecraft. The MISR instrument has been described by Diner, et. al. (1998). MISR views the surface at nine incidence angles (nadir, ±26.1°, ±45.6°, ±60.0°, and ±70.5°) in four spectral filter bandpasses at 446, 558, 672, and 866 nm of bandwidths 42, 29, 22, and 40 nm. The azimuth of MISR's ground track, following an inclination 98.3° depends on latitude. Observations cover a large scattering angle with respect to the sun-surface-sensor, but miss the principal plane in order to avoid sun-glint. Nevertheless, studies have shown that the amount of radiation scattered back towards space can be derived from MISR's discrete-view samples to a high degree of accuracy [Wanner, 1998]. In additional MISR will soon be testing new approaches to the retieval of aerosol abundance and type, and land and cloud morphology [Martonchik, 1998].

Multi-angle viewing sensors, such as MISR, can be used to derive the surface Hemispherical Direction Reflectance Factor (HDRF) and the Bidirectional Reflectance Factor (BRF) [Martonchik, 1994; Abdou et al., 2000]. As described in Bruegge et al. [2000], the HDRF refers to the reflectance properties of the surface, due to the atmosphere and illumination conditions present during a particular measurement campaign. Conversely, the BRF is a fundamental property of the surface alone, is independent of the diffuse sky light contributions, and describes the

are the azimuth and the zenith drives). The motions about the vertical and horizontal axes generates a stepwise pattern in elevation angle increments of 5° and a stepwise pattern in azimuth angle in increments of 5°. An entire scan of both sky and ground hemispheres generates 2664 samples (37 x 72) in about 3.3 minutes. This includes downloading of the angle position data and instrument responses to memory. Figures 2a and 2b show the field-of-view (FOV) projections onto the sky hemisphere, and ground projections, respectively. At the horizon the samples are tangent. These circular FOVs progress towards increasing overlap as the zenith is approached, leading to a varying degree of oversampling. For the ground hemisphere, the pattern is that of elliptical FOVs, increasing in size with increasing view angle from nadir. The ground pattern leads to oversampling at nadir and some undersampling at the horizon. The size of these samples is shown in the figure by comparison to a metric ruler, and represent the projected FOV of PARABOLA when mounted 2 m above the ground.

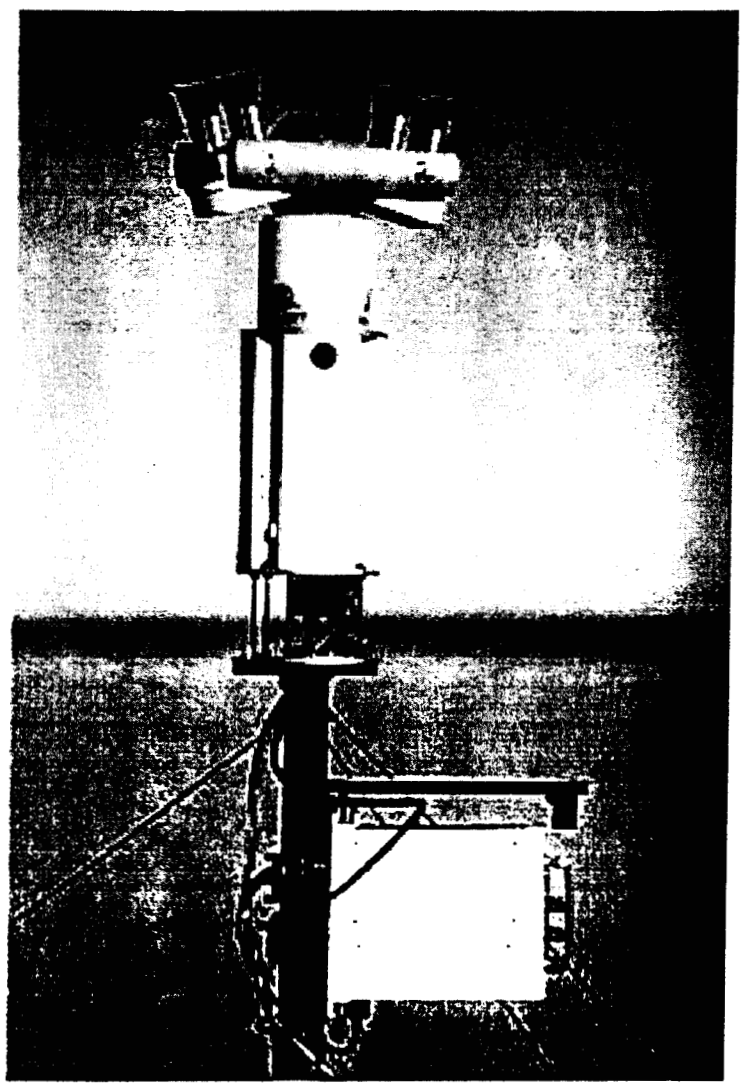

Figure 1. The PARABOLA III scanning radiometer. Shown are the two sensor heads, eight spectrally-filtered radiometers, a reflectance standard, power supply, zip drive housing, and guy-wired stand.

A schematic of the telescope layout is given in Figure 3. The geometric fields of view of each channel are determined by a field stop located in front of the detector plane, and a front entrance aperture located behind the filter. Although the filter is located external to this aperture, it does not restrict or define the field-of-view. This arrangement produces a full-field-of-view (apex at detector center) of 5°, and an annular surrounding zone of partial illumination extending out to full angle of 8°. Three baffles arranged along the telescope tube help to reduce stray light.

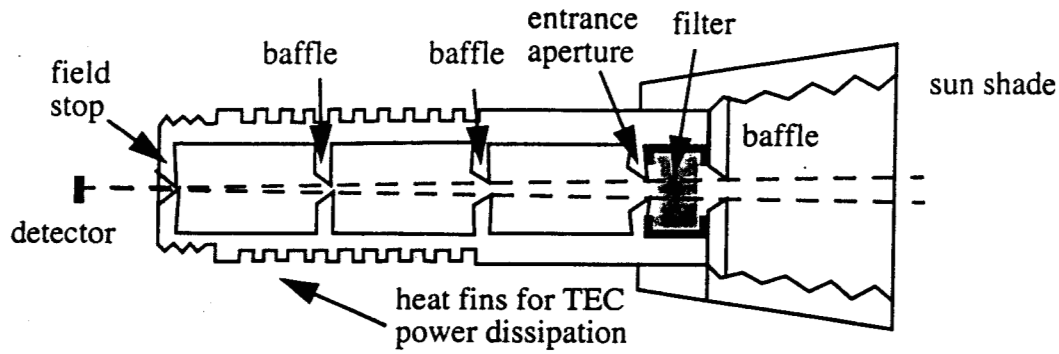

Figure 3. Telescope layout, showing the detector plane, field-defining apertures, baffles, and filter locations.

Three of the four radiometers within each head consist of silicon (Si) detectors; the fourth is made of germanium (Ge), and used for 1030 and 1665 nm detection. Each focal plane is manufactured as a unit, evacuated, and hermetically sealed to allow for detector cooling and to provide protection from the harsh elements where PARABOLA is deployed. The focal plane design is depicted in Figure 4. A cooled transimpediance operational amplifier (op-amp) converts the detector current to a voltage. An external metal-film, thermally insensitive precision resistor which is selected to provide the desired gain. A large dynamic range is allowed, in that a 20 bit analog-to-digital (A/D) converter is used. A separate A/D exists for each of the eight spectral channels, and two 12 bit A/Ds exist for engineering data. To reduce noise, the radiometer A/D converters are mounted directly behind the detector packages. These are operated in parallel, preventing a data bottle-neck which would otherwise ensue.

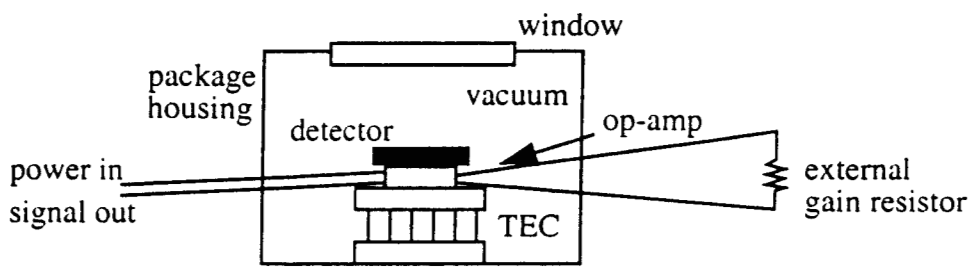

Figure 4. Focal plane layout showing components within hermetic seal.

The detector and op-amp are mounted to the cold side of a thermo-electric cooler (TEC). The temperature is controlled to -10° C. This reduces detector and amplifier noise, and additionally

structures and filename prefixes have been created, continuous data acquisition begins, where data collected are written to the zip cartridge. Several full-day collections can be stored on the zip-cartridge. During the day, the field engineer makes periodic inspections of the instrument during operation, including listening to deviations from its atonal "song". Care is taken to minimize any disturbance to the area.

3. INSTRUMENT CHARACTERIZATION AND CALIBRATION

3.1 Gain determination

As part of a one-time instrument check-out, the JPL PARABOLA was set to track the sun through out a morning, without head rotation. A Langley analysis was then perfomed on these data. That is, a logarithmic form of Beer's law, $\ln (DN)=(-t\ m) + \ln (DN_o/d^2)$, was assumed, and an extrapolation to an airmass, m, of zero was used to determine DNo, the digital number the instrument would produce at the top of atmosphere. (Here DN is the instrument output digital number with the original gain resistor, and d2 the Earth-Sun distance on the day of observation). This analysis was done independently for each channel. In the final step a gain resistor was selected such that saturation was set to a value of 20% above the response to the exo-atmospheric sun:

$$R_{new} = \frac{(2^{20})R_{old}}{1.2DN_o} \qquad (1)$$

3.2 Field-of-view verification

In order to verify the fields-of-view of each of the eight PARABOLA radiometers, a special test was conducted on December 8, 1998. PARABOLA was mounted to a custom tracking mount, which had the capability of providing elevation and azimuth adjustments every 20 seconds. During the course of a morning, the sun was allowed to approach within the PARABOLA fields-of-view. Once the sun became co-aligned with the radiometer axis, the tracker continued to acquire data for some period of time. Following this tracking was shut off, and sun once again slowly moved

Spectral calibration data were acquired in the JPL Standards Laboratory, October 6, 1998. A double pass monochromator was used, an Optronics Laboratories Inc. Model 735IR-D monochromator. The response functions for all channels were determined in the laboratory by illuminating the entrance aperture of each radiometer with a collimated beam of light. The source was a quartz-halogen incandescent lamp, driven from a constant current source. The system is designed to characterize instrument response in the 250 - 3500 nm range. For the 250 to 1100 nm region the monochromator output is monitored by a silicon photodetector; otherwise a germanium photodetector was used. These monitoring signals were used to normalize the actual monochromator output signal such that the response to an effective constant source with wavelength is obtained. Because the monochromator output is weak as compared to the saturation level of PARABOLA, a chopped source/lock-in detection system was used, operating at a chopping frequency of 200 Hz. The electronic output of PARABOLA was detected by picking off the analog signal at the input to the A/D converter for each band. The resulting spectral response functions are shown in Figure 6.

Figure 6. Spectral response functions for the 8 PARABOLA III channels, multiplied by the exo-atmospheric solar irradiance. The dashed lines show the equivalent square band response. Note there is a scale change for the last two channels.

The retrieval of center wavelength and bandwidth proceeds using the same algorithm as used for MISR data reductions [Bruegge, et al., 1998]. We make the assumption that many top-of-atmosphere radiance measurements will have the same relative spectral distribution as the solar spectrum. In our moments analysis, therefore, we weight the camera response function by the exo-atmospheric solar irradiance. The as-built PARABOLA III wavelengths that are quoted are those descriptive of the total-band response region, weighted by the solar spectrum:

$$\lambda_{m,\,solar} = (\int E_{o\lambda} R_\lambda \lambda^2 d\lambda)/(\int E_{o\lambda} R_\lambda \lambda d\lambda) \tag{2}$$

$$\sigma^2 = (\int E_{o\lambda} R_\lambda \lambda^3 d\lambda / \int E_{o\lambda} R_\lambda \lambda d\lambda)(-(\lambda_{m,\,solar})^2) \tag{3}$$

$$\lambda_{u,\,l} = \lambda_{m,\,solar} \pm (\sqrt{3} \cdot \sigma) \tag{4}$$

$$\Delta\lambda_{m,\,solar} = 2\sqrt{3} \cdot \sigma \tag{5}$$

Here the product R_λ is proportional to the sensor response to incident photons; $R_\lambda\,\lambda$ the relative response to a radiance source; m to the moments analysis; and u, and l to the equivalent square band upper and lower wavelength limits, respectively. (More typically, R_λ is used to describe the radiance response, directly. We keep our definition to maintain consistency with our earlier literature). The exo-atmospheric solar irradiance, $E_{o\lambda}$, model used by MISR is one recommended by the EOS calibration panel. The data are published by the World Climate Research Programme [Wehrli, 1985]. Values are reported at 1 astronomical unit (AU).

The results of the spectral analysis are given in Table 1 below. These are reported for a moments analysis done over both the solar-weighted total, and in-band regions. The in-, out-band boundary is defined at the wavelength where the response falls to 1% below peak. It is shown that there are little differences between these parameters, in that PARABOLA has high out-of-band rejection. The out-of-band response is tabulated in the last column, as compute from the out-of-

Table 2. MISR spectral parameters

Total-band		In-band		
center wavelength $\lambda_{m,c}$ (nm)	bandwidth $\Delta\lambda_{m,c}$ (nm)	center wavelength $\lambda_{m,c}^{in-band}$ (nm)	bandwidth $\Delta\lambda_{m,c}^{in-band}$ (nm)	out-of-band response, %
447.5	69.5	446.3	40.9	1
557.8	74.5	557.5	27.2	2-3
669.5	91.9	671.8	20.4	2
857.8	184.2	866.5	38.6	0.8-2

4. RADIOMETRIC CALIBRATION

During radiometric calibration the relationship between an incident radiance field and instrument output is established. The illumination is achieved using an ideal target that emits or reflects unpolarized light, is spatially and angularly uniform, and lacks spectral features such as absorption lines. For this determination PARABOLA made use of a large integrating sphere. The sphere is 1.6 m (65") in diameter, has a 76x23 cm (30x9") exit port, and a 30 cm (12") external satellite sphere with variable aperture. It is sequenced through a number of lamp-on settings, allowing digital data to be collected at radiometric levels evenly spaced within the dynamic range of each spectral channel. The sphere was also used in the preflight calibration of MISR; its size and the calibration procedures were primarily designed to support MISR testing. Difference between MISR and PARABOLA include dynamic range and the location of specific spectral bands. Both MISR and PARABOLA measure downwelling diffuse skylight and surface reflected radiance; only PARABOLA is designed to cover six decades of illumination, thus allowing direct observations of the solar disk. The PARABOLA calibration discussed in this section describes the radiometric response in that portion of the sensor which measures surface reflected radiances. Specifically, the range of equivalent reflectances for which this calibration is valid is roughly between zero and one. Here equivalent reflectance, ρ_{eq}, is a normalized measure of the energy directed towards the camera:

$$\rho_{eq}=L_\lambda \pi / E_{o\lambda} \tag{6}$$

It describes the target reflectance under idealized conditions of illumination (i.e., exo-atmospheric with overhead illumination and the assumption of diffuse reflectance), provides a more intuitive expression of the light levels, and allows instrument properties to be discussed in spectrally independent terms. L_λ is the band-weighted spectral radiance incident on the instrument while observing a target, and $E_{o\lambda}$ is the band-weighted exo-atmospheric solar irradiance at wavelength

To compute the integral required in Eqn. 8, three approaches to the determination of S_λ^{source} were considered. Ideally, a spectrometer would be used to measure the relative spectral output at each output level (i.e., bulb-on combination). This option was not available. A simple estimate of S_λ^{source} can be obtained from the spectral Planck blackbody function at a bulb color temperature of 3100 K, normalized by the value of this function at wavelength b. (The temperature value is provided by the sphere vendor). We elected, however, to use a sphere model, rather than a simple blackbody distribution at a single bulb-color temperature. This model comes from integrating sphere theory, and was provided by the vendor.

Let the output of the main sphere, computed as a function of bulb-type, W, be described by:

$$L_\lambda^{main}(W) = \frac{\eta \cdot \Phi(W)}{\sigma \cdot (T(W))^4} \cdot \frac{\rho_\lambda}{1-\rho_\lambda(1-f)} \cdot \frac{P_\lambda}{\pi A_s} \tag{10}$$

where W refers to the wattage of the bulbs, $\Phi(W)$ = 30 or 200 watts and T(W), the filament temperature, is 3100 and 3220 respectively. The MISR sphere also has a satellite sphere which sits on top of the main sphere. A variable aperture opens or closes to let light from the satellite sphere add to that of the main sphere. The satellite sphere output radiance is described by:

$$L_\lambda^{sat} = \frac{\eta \cdot \Phi(200)}{\sigma \cdot (T(200))^4} \cdot \frac{\rho_\lambda}{1-\rho_\lambda(1-f)} \cdot \frac{\rho_\lambda \cdot V \cdot P_\lambda}{\pi A_s(1-\rho_\lambda(1-f_{sat}))} \quad . \tag{11}$$

Thus, for each of the bulb-on combinations used in the test, n, the total sphere output radiance is given by:

$$L_\lambda^{model}(n) = N(30, n) \cdot L_\lambda^{main}(30) + N(200, n) \cdot L_\lambda^{main}(200) + V_a(n) \cdot L_\lambda^{sat}, \tag{12}$$

where N(W,n) is the number of bulbs turned on at a given level, n, and V_a is the variable aperture of the satellite sphere, a value between 0 and 1.

Other variables in the above equations are:

η = bulb electrical to optical conversion efficiency;

Φ = electrical wattage, either 200W or 30W;

σT^4 = total optical bulb output, integrated over wavelength, σ = 5.67e-20 (W μm^{-2} K^{-4});

ρ = sphere reflectance, for Spectraflec, 0.98 for $\lambda < 670$ nm, 0.966 for $\lambda > 865$ nm with a linear fit between these values for 670 nm $< \lambda <$ 865 nm;

f = 0.05, ratio of non-reflecting area of sphere to total sphere area;

$$G_1 = G_{1m} / k$$

$$G_2 = G_{2m} / k^2.$$

Data from PARABOLA were collected on January 23, 1998, in the MISR highbay. The resulting gain coefficients are tabluated in Table 3. Also tabluated is the constant k, which converts from monochromatic to band-weighted PARABOLA radiances.

Table 3. Band-weighted gain coefficients for PARABOLA 23Jan98 calibration

wavelength, nm	k	G_0 (DN)	G_1 (DN / (W m^{-2} μm^{-1} sr^{-1}))	G_2 (DN / (W m^{-2} μm^{-1} sr^{-1})^2)
444	1.0	54.19	3.72	-1.37e-04
551	1.0	4.89	4.11	-2.72e-05
581 (PAR)	1.20	45.13	3.36	-2.00e-05
650	1.0	126.75	5.05	-4.10e-04
860	1.0	40.12	6.32	2.87e-04
944	1.0	-186.52	20.61	-8.79e-04
1028	0.645	-3.71	7.87	1.34e-03
1650	0.999	78.25	9.98	3.74e-02

4.1 Radiometric uncertainties

At best, the calibration described above is good to the MISR calibration requirements of 3% absolute uncertainty (1σ level of confidence). This would be true for PARABOLA wavelengths that are close to the photodiode wavelengths, where the wavelength interpolation scaler is close to unity. The uncertainties at these wavelengths have been documented elsewhere [Bruegge, 1998]. We would expect larger uncertainties at PARABOLA wavelengths not covered by the standards.

An opportunity to validate this calibration presented itself, by using data acquired during a June 18-20, 1997 experiment, conducted at the University of Arizona, Tucson. At that time the Optical Science Center measured their sphere radiance, using their portable transfer radiometer. Results from the PARABOLA and UofA radiometers are tabluated in Table 4. This verification

4.2 Dark current

On April 4, 1999, the PARABOLA dark current was monitored over a time period of 72

Table 5. Dark current mean and standard deviations

wavelength, nm	G_0 (DN)	Dark current, DN (initial)	Dark current, DN (after warm-up)	Radiance uncertainty, %, at ρ_{eq}=0.01
444	54.19	56	54	0.69
551	4.89	36	36	25.
581 (PAR)	45.13	67	63	10.
650	126.75	26	-3	13.
860	40.12	68	68	7.4
944	-186.52	205	90	14.
1028	-3.71	21	9	23.
1650	78.25	108	94	3.5

minutes. The range of these data, from initial turn-on, to final warm-up, is given in Table 5. In every instance the dark current drifted slowly and continually during this time window. For comparison, the G_0 coefficient is shown for these wavelengths. In theory, this coefficient should represent the dark current, as derived from our calibration experiment. As a dark reading was not incorporated into the data regression, we see that there is some divergence between the coefficient and the measured dark current readings. In order to assess the impact of this on the radiance product, we have computed the range of values, that is the maximum of the G_0, dark current data values, minus the associated minimum value. To first order the radiance error is inversely proportional to the G_1 coefficient. This radiance error is expressed as a percentage of the radiance, at an input illumination of 0.01 in equivalent reflectance, in the table above. We see the expected uncertainty at such a low signal is as large as 25%. At high illumination levels, this effect becomes negligible (on the order of 0.2% at 1.0 equivalent reflectance). Thus, for retrieval of low-radiances, an improved understanding of the measured dark current both at the time of calibration, and during the data acquisition, is required.

It is important to note that the dark current must also be properly accounted for in circumstances where a reflectance standard is used, rather than the radiometric calibration. This technique, where the DN from PARABOLA while observing a target under study is ratioed to that DN when it observes a panel of known reflectance, is common when surface reflectance is desired. Using an dark illumination input of 0.01 equivalent reflectance, the percentage error is computed to be 60%, if the dark current is not first subtracted prior to making the ratio. This is because the dark current, as reported in Table 5, is a significant portion of the signal recorded under low-illumination conditions. Even for very bright surfaces the dark current cannot be ignored (the error in doing so is reduced to 1% at an equivalent reflectance of 1.)

Deering, D.W. and P. Leone, A sphere-scanning radiometer for rapid directional measurements of sky and ground radiance, Remote Sens. of Environ. 19:1- 24, 1986.

Diner, David J., Gregory P. Asner, Roger Davies, Yuri Knyazikhin, Jan-Peter Muller, Anne W. Nolin, Bernard Pinty, Crystal B. Schaaf, and Julienne Stroeve, New directions in Earth Observing: Scientific applications of multi-angle remote sensing, Bull. Am. Meteorol. Soc., 80(11), 2209-2228, November 1999.

Diner, D.J., J.C. Beckert, T.H. Reilly, C.J. Bruegge, J.E. Conel, R. Kahn, J.V. Martonchik, T.P. Ackerman, R. Davies, S.A.W. Gerstl, H.R. Gordon, J-P. Muller, R. Myneni, R.J. Sellers, B. Pinty, and M.M. Verstraete, Multiangle Imaging SpectroRadiometer (MISR) description and experiment overview, IEEE Trans. Geosci. Rem. Sens., Vol. 36, 1072-1087, 1998.

Korechoff, R.P., D. Kirby, E. Hochberg, C. Sepulveda, and V. Jovanovic, Distortion calibration of the MISR linear detectors, in *Earth Observing System*, Proc. SPIE, Vol. **2820**, Denver, 5-9 August 1996.

Martonchik, J.V., D.J. Diner, R. Kahn, T.P. Ackerman, M.M. Verstraete, B. Pinty, and H.R. Gordon, Techniques for the retrieval of aerosol properties over land and ocean using multi-angle imaging, IEEE Trans. Geosci. Rem. Sens., Vol. 36, pp. 1212-1227, 1998.

Wanner, Wolfgang, Expected retrieval accuracies of bidirectional reflectance and albedo from EOS-MODIS and MISR angular sampling, J. Geophys. Res. 1998.

Wehrli, C., Extraterrestrial Solar Spectrum, World Radiation Center (WRC), Davos-Dorf, Switzerland, WRC Publication No. 615, July 1985.